Partial widths from analytical extension of the wave function: P_c states

Zi-Yang Lin,[*] Jian-Bo Cheng,[†] Bo-Lin Huang,[‡] and Shi-Lin Zhu[§]
School of Physics and Center of High Energy Physics, Peking University 10087, China

(Received 19 June 2023; revised 24 June 2023; accepted 16 November 2023; published 14 December 2023)

A new approach to partial widths is proposed through the analytical extension of the wave function in momentum space. By including the residue of the wave function, the Schrödinger equation is extended to the second Riemann sheet. As a result, the partial width is associated with the pole of the wave function. The resonance wave function is convergent in momentum space and can be used to evaluate other observables. This approach is applied to a coupled-channel analysis for P_c states, involving the contact interactions and one-pion-exchange potential with the three-body effects. Under the reasonable assumption that the off-diagonal contact interactions are small, the J^P quantum numbers of the $P_c(4440)$ and the $P_c(4457)$ are $\frac{1}{2}^-$ and $\frac{3}{2}^-$ respectively. The low energy constants are fitted using the experimental masses and widths as input. The $P_c(4312)$ is found to decay mainly to $\Lambda_c\bar{D}^*$, while the branching ratios of the $P_c(4440)$ and $P_c(4457)$ in different channels are comparable. Three additional P_c states at 4380 MeV, 4504 MeV and 4516 MeV, together with their branching ratios, are predicted. Additionally, a deduction for the revised one-pion-exchange potential involving the on-shell three-body intermediate states is provided.

DOI: 10.1103/PhysRevD.108.114014

I. INTRODUCTION

Searching for exotic states composed of four or more quarks has been a hot topic in hadron physics [1–8]. Since the discovery of the hidden-charm pentaquarks, the P_c states, (also named as P_ψ^N in line with the new naming convention for the exotic states [9]), have been investigated in a variety of works. Although the P_c states are commonly believed to be the bound states of the charmed mesons and baryons, only their masses or binding energies can be obtained from the Schrödinger equation. In this work, we aim to derive their branching ratios in the open-charm channels, together with their masses and total widths in a self-consist framework. We apply the complex scaling method (CSM) to a coupled-channel analysis and explain how the analytical extension of the wave function works. Besides, we include the effect of the on-shell three-body intermediate states.

The $P_c(4380)$ and $P_c(4450)$ states were first observed in the $J/\psi p$ invariant mass spectrum in the $\Lambda_b^0 \to J/\psi p K^-$ decays by the LHCb Collaboration in 2015 [10,11]. They carried out a more precise analysis with a larger data sample in 2019, and discovered a new state $P_c(4312)$ and the two peak structure of the $P_c(4450)$, namely $P_c(4440)$ and $P_c(4457)$ [12]. Their masses and widths are listed in Table I, which are fitted under the incoherent relativistic Breit-Wigner assumptions. Additionally, the evidence of a new structure $P_c(4337)$ was found in the $B_s^0 \to J/\psi p\bar{p}$ decays in 2021 [13].

These pentaquarks lie close to and below the $\Sigma_c^{(*)}\bar{D}^{(*)}$ thresholds, and are commonly believed to be the hadronic molecules, which were first predicted in Refs. [14–16]. Since their discovery, they have been investigated in the frameworks of the quark model [17,18], kinematical effects [19–21], compact states coupled to the meson-hadron channels [22], the QCD sum rule [23], the vector-meson-exchange model [24,25], the one-boson-exchange model [26], the large N_c approximation [27] and the chiral effective field theory [28,29]. (For a detailed review, see Refs. [5,6,8] and the review "pentaquark" in Ref. [30]). The P_c states have also been investigated by lattice QCD in charmonium-nucleon systems [31,32]. Recently, the P_c states are first observed on lattice in $\Sigma_c\bar{D}$ and $\Sigma_c\bar{D}^*$ channels [33].

TABLE I. The P_c states reported in Ref. [12].

State	M(MeV)	Γ(MeV)
$P_c(4312)^+$	$4311.9 \pm 0.7^{+6.8}_{-0.6}$	$9.8 \pm 2.7^{+3.7}_{-4.5}$
$P_c(4440)^+$	$4440.3 \pm 1.3^{+4.1}_{-4.7}$	$20.6 \pm 4.9^{+8.7}_{-10.1}$
$P_c(4457)^+$	$4457.3 \pm 0.6^{+4.1}_{-1.7}$	$6.4 \pm 2.0^{+5.7}_{-1.9}$

[*]lzy_15@pku.edu.cn
[†]jbcheng@pku.edu.cn
[‡]blhuang@pku.edu.cn
[§]zhusl@pku.edu.cn

Since the pion exchanges provide a strong coupling between the $\Sigma_c^{(*)}\bar{D}^{(*)}$ channels, a coupled-channel analysis is required in the molecule picture. In two-body coupled-channel scatterings, the T matrix or the S matrix appears as a multivalued function of the center-of-mass energy. The Riemann sheets are classified by the imaginary parts of the momenta in the corresponding channels. The Riemann sheet corresponding to the momentum with a positive imaginary part is called the first (physical) sheet, and the Riemann sheet corresponding to the momentum with a negative imaginary part is called the second (unphysical) sheet. Resonances and bound states, which are poles of the T matrix, are distributed on these Riemann sheets. Among them only the poles near the physical region significantly affect the cross section. The P_c states are most likely to be the quasi-bound states (Feshbach resonances). They are on the first Riemann sheet with respect to the higher thresholds and on the second Riemann sheet with respect to the lower thresholds, which is also referred to as "proximal" Riemann sheet. Poles on these sheets usually cause bumplike resonances seen in the cross section. In a coupled-channel analysis, the two-body open-charm decay widths will be obtained automatically. In Refs. [34–37], the widths and T matrix residues of the P_c states are obtained through the Bethe-Salpeter equation or the Lippmann-Schwinger equation (LS equation).

The three-body effect should be taken into account since the mass difference between the $D(\Lambda_c)$ and $D^*(\Sigma_c)$ is comparable to the pion mass. The large transferred energy of the exchanged pion results in a retarded potential in coordinate space. Besides, the intermediate $\Lambda_c\bar{D}\pi$ state can be on-shell and contribute to the total width. In Ref. [38], the authors discussed the three-body effect and the consequent left-hand or right-hand cut in the T_{cc}^+ state. When the mass difference is larger than the pion mass, the one-pion-exchange (OPE) potential introduces a right-hand cut at the three-body threshold and the quasibound state lies on the second Riemann sheet with respect to the three-body threshold. In Ref. [36,39], the authors calculated the pole positions and couplings of the P_c states in the framework of the time-ordered-perturbation theory and the LS equation. In this work, we retain both the relativistic form and the three-body effect in the OPE potential and adopt the complex scaling method (CSM).

The CSM is a shortcut to derive the bound states and resonances simultaneously by extending the Schrödinger equation to the complex plane [40,41]. In Ref. [42], we put forward the CSM in momentum space to investigate the T_{cc}^+ and $X(3872)$. In this work, we further study the complex wave function and develop the partial width formula. Moreover, we systematically illustrate the CSM in momentum space from the point of view of analytical extension. In principle, with an appropriate choice of the integral path, we can solve the poles of the T matrix on any Riemann sheets. Similar transformations can be employed in LS equations [43].

This paper is organized as follows. In Sec. II, we introduce the Lagrangians including the OPE and contact terms. In Secs. III and IV, we explain the CSM in momentum space and its application to calculate the partial width. In Sec. V, we derive the OPE potential involving the three-body effect. Then in Sec. VI, we present the parameters and effective potentials. In Sec. VII, we fit the low energy constants (LEC) using the masses and widths of the $P_c(4312)$, $P_c(4440)$ and $P_c(4457)$ as inputs and predict their branching ratios in the open-charm channels. We predict several states. Section VIII is a summary.

II. LAGRANGIAN

We interpret the $P_c(4312)$, $P_c(4440)$, and $P_c(4457)$ as the $\Sigma_c\bar{D}^{(*)}$ molecules. A coupled-channel analysis is performed in the $\Sigma_c^{(*)}\bar{D}^{(*)}$ system. The Lagrangian is constructed under heavy quark spin symmetry (HQSS) [44]. The leading order contact terms and OPE are included.

Following Refs. [29,45], we organize the Λ_c and $\Sigma_c^{(*)}$ states into an isosinglet and an isotriplet. The matrices in $SU(2)$ flavor space read

$$\psi_1 = \begin{bmatrix} 0 & \Lambda_c^+ \\ -\Lambda_c^+ & 0 \end{bmatrix}, \quad \psi_3 = \begin{bmatrix} \Sigma_c^{++} & \frac{\Sigma_c^+}{\sqrt{2}} \\ \frac{\Sigma_c^+}{\sqrt{2}} & \Sigma_c^0 \end{bmatrix}, \quad \psi_{3^*}^\mu = \begin{bmatrix} \Sigma_c^{*++} & \frac{\Sigma_c^{*+}}{\sqrt{2}} \\ \frac{\Sigma_c^{*+}}{\sqrt{2}} & \Sigma_c^{*0} \end{bmatrix}^\mu, \tag{1}$$

where "1" denotes the iso-singlet, and "3" denote the isotriplet. The $\psi_{3^*}^\mu$ denotes the spin-$\frac{3}{2}$ Rarita-Schwinger field.

The Σ_c and Σ_c^* form a multiplet under HQSS, which can be arranged into a superfield,

$$\begin{aligned} \psi^\mu &= \mathcal{B}_{3^*}^\mu - \frac{1}{\sqrt{3}}(\gamma^\mu + v^\mu)\gamma^5\mathcal{B}_3, \\ \bar{\psi}^\mu &= \bar{\mathcal{B}}_{3^*}^\mu + \frac{1}{\sqrt{3}}\bar{\mathcal{B}}_3\gamma^5(\gamma^\mu + v^\mu), \end{aligned} \tag{2}$$

where $\mathcal{B}_i$ $(i = 1, 3, 3^*)$ is the light components of the heavy baryon fields,

$$\mathcal{B}_i = e^{iM_i v\cdot x}\frac{1+\not{v}}{2}\psi_i, \qquad \mathcal{H}_i = e^{iM_i v\cdot x}\frac{1-\not{v}}{2}\psi_i. \tag{3}$$

Under the heavy quark symmetry, only the light components with the projection operator $\frac{1+\not{v}}{2}$ survive in the leading order. The heavy components only contribute to $1/M_Q$ corrections and vanish when the heavy quark mass $M_Q \to \infty$. Considering the $SU(2)$ chiral symmetry in flavor space, the LO Lagrangian reads,

$$\mathcal{L}_{\mathcal{B}\phi} = -\mathrm{Tr}(\bar{\psi}^\mu i v\cdot D\psi^\mu) + \frac{i\delta_a}{2}\mathrm{Tr}(\bar{\psi}^\mu\sigma_{\mu\nu}\psi^\nu) + ig_1\epsilon_{\mu\nu\rho\sigma}\mathrm{Tr}(\bar{\psi}^\mu u^\rho v^\sigma\psi_\nu) + g_2\mathrm{Tr}(\bar{\psi}^\mu u_\mu\mathcal{B}_1 + \mathrm{H.c.}), \tag{4}$$

where the covariant derivative is $D_\mu = \partial_\mu + i\Gamma_\mu$, and δ_a introduces the mass splitting between the Σ_c and the Σ_c^*. Γ_μ and u_μ denotes the chiral connection (vector current) and the axial current of Goldstone boson fields,

$$\begin{aligned}\Gamma_\mu &= \frac{i}{2}[\xi^\dagger,\partial_\mu\xi] = -\frac{1}{4f_\pi^2}\epsilon^{abc}\tau^c(\phi^a\partial_\mu\phi^b) + \cdots,\\ u_\mu &= \frac{i}{2}\{\xi^\dagger,\partial_\mu\xi\} = -\frac{1}{2f_\pi}\tau^a\partial_\mu\phi^a + \cdots,\\ \xi &= \exp(i\phi/2f_\pi),\\ \phi &= \phi^a\tau^a = \sqrt{2}\begin{pmatrix}\frac{\pi^0}{\sqrt{2}} & \pi^+\\ \pi^- & -\frac{\pi^0}{\sqrt{2}}\end{pmatrix},\end{aligned} \tag{5}$$

where ϕ denotes the Goldstone boson field, τ^a denotes the Pauli matrices in $SU(2)$ flavor space, and $f_\pi = 92$ MeV stands for the pion decay constant.

Noticing that the total spin of light quarks in the superfield is either 0 or 1, the spinor part of the superfield corresponds to the spin of the heavy quark. Terms such as $\bar{\psi}^\mu\not{v}\psi_\mu$ and $\bar{\psi}^\mu\sigma^{\nu\rho}u_\nu v_\rho\psi_\mu$ are forbidden in the leading order, since the gamma matrices break the HQSS. In principle, there are only two independent coupling constants g_1 and g_2 in Eq. (4). In previous works [28,46], they are usually related using quark models, and g_2 can be evaluated from the $\Sigma_c^{(*)} \to \Lambda_c\pi$ decay,

$$g_1 = -1.47 = -\sqrt{2}g_2, \qquad g_2 = 1.04. \tag{6}$$

The Lagrangians for the $\bar{D}^{(*)}$ sector can be constructed similarly. The superfield $\tilde{H}$ for $\bar{D}^{(*)}$ reads

$$\begin{aligned}\tilde{H} &= (\tilde{P}_\mu^*\gamma^\mu + i\tilde{P}\gamma_5)\frac{1-\not{v}}{2},\\ \bar{\tilde{H}} &= \gamma^0 H^\dagger\gamma^0 = \frac{1-\not{v}}{2}(\tilde{P}_\mu^{*\dagger}\gamma^\mu + i\tilde{P}^\dagger\gamma_5),\\ \tilde{P} &= \begin{pmatrix}\bar{D}^0\\ D^-\end{pmatrix}, \qquad \tilde{P}_\mu^* = \begin{pmatrix}\bar{D}^{*0}\\ D^{*-}\end{pmatrix}.\end{aligned} \tag{7}$$

Then the LO Lagrangian for the $\bar{D}^{(*)}\pi$ interaction reads

$$\mathcal{L}_{\tilde{H}\phi} = -\langle(iv\cdot D\bar{\tilde{H}})\tilde{H}\rangle - \frac{1}{8}\delta\langle\bar{\tilde{H}}\sigma^{\mu\nu}\tilde{H}\sigma_{\mu\nu}\rangle + g\langle\bar{\tilde{H}}\not{v}\gamma_5\tilde{H}\rangle. \tag{8}$$

Apart from the OPE potential, contact terms are required to mimic the short-range interactions. There are six independent terms in the LO Lagrangian since the gamma matrices, which are related to the spin of the heavy quark, are not allowed,

$$\mathcal{L}_{\mathcal{B}H} = C_1\langle\bar{\tilde{H}}\tilde{H}\rangle\mathrm{Tr}(\bar{\mathcal{B}}_1\mathcal{B}_1) + C_2\langle\bar{\tilde{H}}\gamma^\mu\gamma^5\tau^a\tilde{H}\rangle\mathrm{Tr}(\bar{\mathcal{B}}_1\tau^a\psi_\mu) + \mathrm{H.c.} \tag{9}$$

$$+ C_3\langle\bar{\tilde{H}}\tilde{H}\rangle\mathrm{Tr}(\bar{\psi}^\mu\psi_\mu) + iC_4\epsilon_{\sigma\mu\nu\rho}v^\sigma\langle\bar{\tilde{H}}\gamma^\rho\gamma^5\tilde{H}\rangle\mathrm{Tr}(\bar{\psi}^\mu\psi^\nu) \tag{10}$$

$$+ C_5\langle\bar{\tilde{H}}\tau^a\tilde{H}\rangle\mathrm{Tr}(\bar{\psi}^\mu\tau^a\psi_\mu) + iC_6\epsilon_{\sigma\mu\nu\rho}v^\sigma\langle\bar{\tilde{H}}\gamma^\rho\gamma^5\tau^a\tilde{H}\rangle\mathrm{Tr}(\bar{\psi}^\mu\tau^a\psi^\nu), \tag{11}$$

where $\langle\cdots\rangle$ stands for the trace in spinor space and $\mathrm{Tr}(\cdots)$ stands for the trace in flavor space. The $C_3(C_4)$ and $C_5(C_6)$ terms differ only by an isospin factor. Since we focus on the $I = \frac{1}{2}$ case, there are only four independent terms.

III. COMPLEX SCALING METHOD

We use CSM to search for the possible bound states or resonances. The CSM is an analytical extension of the Schrödinger equation, proposed by Aguilar, Balslev, and Combes [47,48]. For a two-body scattering process, it is equivalent to the nonrelativistic LS equation.

We start from the Schrödinger equation in momentum space

$$E\phi_l(p) = \frac{p^2}{2m}\phi_l(p) + \int\frac{p'^2dp'}{(2\pi)^3}V_{l,l'}(p,p')\phi_{l'}(p'), \tag{12}$$

where l, l' are quantum numbers of the orbital angular momenta, and p denotes the momentum in the center-of-mass frame. The corresponding LS equation reads

$$T(k',k;k_0) = V(k',k) + \int_0^\infty\frac{p^2dp}{(2\pi)^3}\frac{V(k',p)T(p,k;k_0)}{E_{k_0} - E_p + i0+}, \tag{13}$$

where $E_{k_0} = \frac{k_0^2}{2m}$, $E_p = \frac{p^2}{2m}$ are the nonrelativistic kinetic energies.

With a complex scaling operation on Eq. (12), $p \to pe^{-i\theta}$, $\tilde{\phi}_l(p) = \phi_l(pe^{-i\theta})$, which will not change the eigenenergy E, we derive the complex scaled Schrödinger equation with a scaling angle θ,

$$E\tilde{\phi}_l(p) = \frac{p^2e^{-2i\theta}}{2m}\tilde{\phi}_l(p) + \int\frac{p'^2e^{-3i\theta}dp'}{(2\pi)^3} \times V_{l,l'}(pe^{-i\theta},p'e^{-i\theta})\tilde{\phi}_{l'}(p'). \tag{14}$$

An equivalent complex scaling operation in coordinate space will make the resonance wave functions convergent at $r \to \infty$. This can be roughly understood from the point of view of the asymptotic wave function

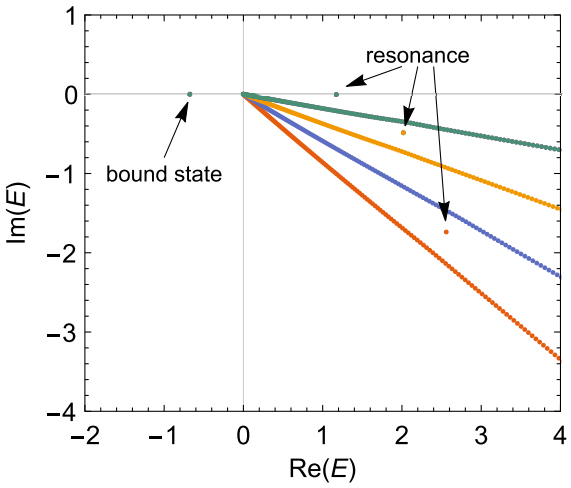

FIG. 1. A typical solution of the complex scaled Schrödinger equation. Eigenenergies are plotted on the complex plane. The continuum states line up due to the same arguments $\mathrm{Arg}(E) = -2\theta$. Points with different colors stand for eigenenergies solved under different θ. With a Hermitian Hamiltonian, the bound states lie on the negative real axis, while the resonances lie on the fourth quadrant, and appear only when $|\mathrm{Arg}(E)| < 2\theta$.

$$\psi(r) \xrightarrow{r\to\infty} f_l^+(k)e^{-ikr} + f_l^-(k)e^{ikr}, \xrightarrow{r\to r\exp(i\theta)} f_l^+(k)e^{-ikre^{i\theta}} + f_l^-(k)e^{ikre^{i\theta}}, \quad (15)$$

where $f_l^{\pm}(k)$ are Jost functions. Resonances and bound states correspond to the poles of the T matrix, or the zeros of $f_l^+(k)$. The first term vanishes and the second term converges when $\mathrm{Arg}k_{\mathrm{res}} > -\theta$. However, we stress that this is an inaccurate explanation since the asymptotic form is obtained assuming r is real, and in general, cannot be extended to the whole complex plane [49]. A strict analytical form of the wave function in coordinate space is obtained in Eq. (22). As explained in Sec. IV, whether the divergent term shows up depends on the integral path and the poles of the wave function.

A typical distribution of the eigenenergies solved by the CSM is shown in Fig. 1. The continuum states line up and rotate as the complex scaling angle θ varies. Poles are isolated from the continuum states. The region between the continuum line and $+x$-axis corresponds the second Riemann sheet and is where the resonances lie. The rest of the complex plane corresponds to the 1st Riemann sheet and is where the bound states lie.

In the coupled-channel cases, only the bound states below the lowest channel can be directly solved in the normal Schrödinger equation [Eq. (12)]. For a "bound state" coupling to an open channel with a lower threshold, its wave function of the lower channel will be divergent, and thus cannot be solved. Poles of this type lie on the 1st Riemann sheet of the higher channel, and the second Riemann sheet of the lower channel. They are called the quasibound states, Feshbach-type resonances or unstable bound states. Using CSM, both their energies and widths can be solved directly from Eq. (14). For a more precise classification of the poles, see Ref. [50].

IV. ANALYTICAL EXTENSION OF WAVE FUNCTION AND PARTIAL WIDTHS

Since the complex scaled Schrödinger equation is equivalent to the LS equation, we can dig out the information of the T matrix at the resonance energy E_{res} from the corresponding resonance wave function. We will present an approach to calculate the residues of the T matrix, which corresponds to the partial widths of the states under the narrow resonance approximation. There are several previous works dealing with the partial widths using CSM [51,52]. Our approach is derived in momentum space without extra approximations.

The complex scaled wave function $\tilde{\psi}(r)$ solved from Eq. (14) is indeed an analytical extension of the real wave function $\psi(r)$ solved from Eq. (12). They are associated through the Schrödinger equation,

$$\langle k|\hat{T} + \hat{V}|\phi\rangle = E_R\langle k|\phi\rangle, \quad (16)$$

where $\hat{T}$, $\hat{V}$ denotes the kinetic energy and the potential, respectively, and the $E_R = M - i\frac{\Gamma}{2}$ is the resonance energy.

In the momentum presentation, we obtain

$$\frac{\boldsymbol{k}^2}{2m}\phi(\boldsymbol{k}) + \int \frac{d^3\boldsymbol{p}}{(2\pi)^3} V(\boldsymbol{k},\boldsymbol{p})\phi(\boldsymbol{p}) = E_R\phi(\boldsymbol{k}), \quad (17)$$

or

$$\phi(\boldsymbol{k}) = \frac{1}{E_R - \frac{\boldsymbol{k}^2}{2m}} \int \frac{d^3\boldsymbol{p}}{(2\pi)^3} V(\boldsymbol{k},\boldsymbol{p})\phi(\boldsymbol{p}), \quad (18)$$

where $\boldsymbol{k}$ can be set to be any complex value, while $\boldsymbol{p}$ is always real as long as we carry out the integral along the real axis. Then we can extend the wave function to the complex plane once we obtain the wave function on the position real axis.

Furthermore, we can employ a complex scaling operation and derive

$$\phi(\boldsymbol{k}) = \frac{1}{E_R - \frac{\boldsymbol{k}^2}{2m}} \int \frac{d^3\boldsymbol{p}}{(2\pi)^3} e^{-3i\theta} V(\boldsymbol{k},\boldsymbol{p}e^{-i\theta})\tilde{\phi}(\boldsymbol{p}), \quad (19)$$

where $\tilde{\phi}(\boldsymbol{p}) = \phi(\boldsymbol{p}e^{-i\theta})$.

The complex scaling operation is not always feasible since it requires $\lim_{p\to\infty} p^3 V_{l,l'}(k,p)\phi(p) \to 0$. Here we assume it to be true since the potential usually contains a cutoff at large momenta. But it constrains the range of the complex scaling angle θ, because the potential $V_{l,l'}(k,p)$ is always accompanied by some nonanalytical behaviors

(unless it is a constant). For example, a monopole or dipole regulator $1/(q^2+\Lambda^2)^n$ introduces a left-hand cut to the potential after the partial wave expansion, and an exponential regulator $\exp(-q^n/\Lambda^n)$ introduces a singularity at infinity, which sets the constraint $\theta < \pi/(2n)$ to avoid divergence.

From Eq. (19), we see that $\phi(k)$ diverges at $k = \pm\sqrt{2mE_R}$. This applies to both the bound states and resonances in the scattering problems, in which the potential satisfies

$$\lim_{r\to\infty} r^2 V(r) \to 0. \tag{20}$$

The poles of the wave function result in discontinuity of the integral. (See Fig. 5 in Sec. V as an example.) In Eq. (14) and Eq. (19), the integral paths above and below the pole differ by the residue of the pole. Whether we take into account the contribution of the pole in the integral determines the type of the state. For a resonance on the second Riemann sheet, the integral should be performed below the pole.

Then we focus on the wave function in coordinate space, which is related to the wave function in momentum space through the Fourier transformation

$$\psi_l(r) = \int_0^\infty \frac{4\pi p^2 dp}{(2\pi)^3} e^{-3i\theta}\phi_l(pe^{-i\theta}) i^l j_l(pre^{-i\theta}), \tag{21}$$

where j_l is the lth spherical Bessel function, which is divergent at $p\to\infty$ when $0<\theta<\pi$. If we change the integral path to $\theta = 0$ then we have to add the residue of the pole to compensate for the discontinuity

$$\begin{aligned}\psi_l(r) &= \int_0^\infty \frac{4\pi p^2}{(2\pi)^3}\phi_l(p) i^l j_l(pr) dp \\ &\quad + 2\pi i \mathrm{Res}\left\{\frac{4\pi p^2}{(2\pi)^3}\phi_l(p) i^l j_l(pr)\right\}\Big|_{p=k_R} \\ &= \int_0^\infty \frac{4\pi p^2}{(2\pi)^3}\phi_l(p) i^l j_l(pr) dp \\ &\quad + i^{l+1}\frac{k_R^2}{\pi} j_l(k_R r) \lim_{p\to k_R}(p-k_R)\phi_l(p),\end{aligned} \tag{22}$$

where $k_R = \sqrt{2mE_R}$.

The first term in Eq. (22) is convergent at $r\to\infty$, and the second term gives the asymptotic behavior of $\psi_l(r)$ at $r\to\infty$,

$$\psi_l(r) \to \frac{i^l k_R}{2\pi}\lim_{p\to k_R}(p-k_R)\phi_l(p)\frac{e^{i(k_R r-\pi l/2)}}{r}, \tag{23}$$

which diverges when k_R is not real. If we employ a transformation $r\to re^{i\theta}$, then we have to replace $p\to pe^{-i\theta}$ in the integral to keep $j_l(pr)$ convergent at $r\to\infty$.

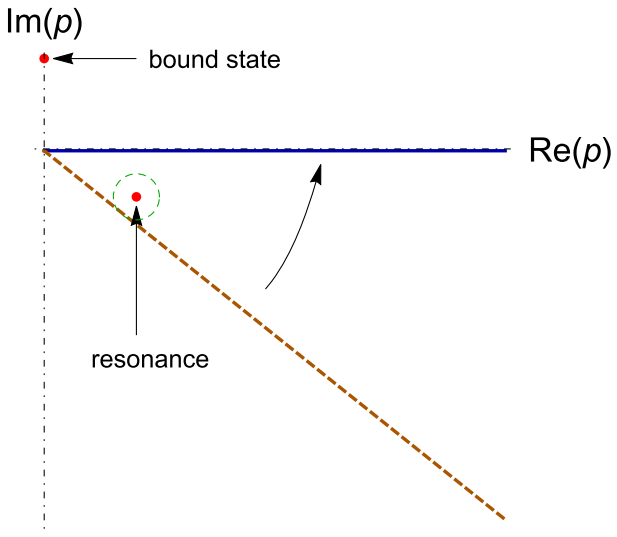

FIG. 2. The differences between the poles on the 1st and 2nd Riemann sheets. Integrals along the brown dashed line and the blue solid line are equal for the bound states, but different for the resonances. The correct choice of the integral paths for the resonances is the brown dashed line, which corresponds to the equation on the 2nd Riemann sheet. For the resonances, if we change the integral path to the blue solid one, then we need an additional integral path along the green dashed circle for compensation, which corresponds to the residue of the pole.

When the integral path passes the pole, the second term vanishes and the wave function becomes convergent.

In multichannel cases, the wave function of the jth channel satisfies

$$\psi_{l,j}(r) \to \frac{i^l k_{R,j}}{2\pi}\lim_{p\to k_{R,j}}(p-k_{R,j})\phi_{l,j}(p)\frac{e^{i(k_{R,j}r-\pi l/2)}}{r}. \tag{24}$$

where $k_{R,j} = \sqrt{2m_j(E_R - E_{\mathrm{th},j})}$, m_j and $E_{\mathrm{th},j}$ are the (reduced) mass and the threshold of the i-th channel.

We stress that Eq. (22) applies only to the poles on the 2nd Riemann sheet. For the poles on the 1st Riemann sheet, the pole will not cross the integral path when θ varies to zero. As shown in Fig. 2, for a pole on the 1st Riemann sheet, the integral path can be rotated continuously from θ to 0. So the second term in Eq. (22) vanishes. The wave function tends to 0 as $r\to\infty$. In other words, the state will not decay to this channel. When calculating the partial widths, we only need to consider the channels in which the pole is on the 2nd Riemann sheet, no matter whether the resonance energy is above or below the threshold. Notably, $k_{R,j}$ is usually complex and $k_{R,j}$ in different channels can be quite different.

The coefficients of the spherical wave in different channels correspond to the component proportions of the outgoing state. It represents the amplitudes of decaying to different final states and is related to the branching ratios of the resonance. It is not the modulus of

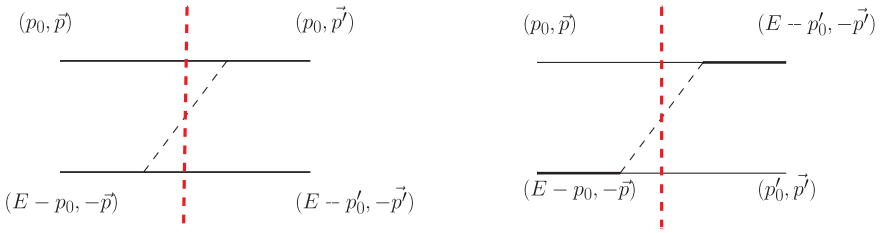

FIG. 3. The one-pion-exchange diagram. Left: direct diagram (P_c); Right: cross diagram (T_{cc}^+). E denotes the center-of-mass energy. The on-shell intermediate state contributes to the imaginary part.

the wave function but the residue of the wave function at the resonance energy that determines the branching ratios. Following the formula derived by Moiseyev and Peskin [53], we obtain

$$\frac{\Gamma_1}{\Gamma_2}=\left|\frac{k_{R,1}/\mu_1}{k_{R,2}/\mu_2}\right|\left|\frac{k_{R,1}\lim_{p\to k_{R,1}}(p-k_{R,1})\phi_1(p)}{k_{R,2}\lim_{p\to k_{R,2}}(p-k_{R,2})\phi_2(p)}\right|^2. \quad (25)$$

Directly calculating the residue of the wave function may yield a large numerical error, so we use an alternative approach. Noticing that the residue of $\phi(p)$ at $p=k_R$ can be calculated through Eq. (19) by letting $k\to k_R$, we finally derive

$$\frac{\Gamma_1}{\Gamma_2}=\left|\frac{k_{R,1}\mu_1}{k_{R,2}\mu_2}\right|\left|\frac{\langle k_{R,1}|\hat{V}|\phi\rangle}{\langle k_{R,2}|\hat{V}|\phi\rangle}\right|^2, \quad (26)$$

where

$$\langle k_{R,j}|\hat{V}|\phi\rangle=\int\frac{p^2dp}{(2\pi)^3}e^{-3i\theta}V_{jm}(k_{R,j},pe^{-i\theta})\tilde{\phi}_m(p), \quad (27)$$

where j, m are the channel labels.

If we choose the normalization condition defined by c-product [54], which reads

$$(\phi|\phi)=\int\frac{d^3\boldsymbol{k}}{(2\pi)^3}\phi(k)^2=\int\frac{d^3\boldsymbol{k}}{(2\pi)^3}e^{-3i\theta}\phi(ke^{-i\theta})^2=1, \quad (28)$$

then the expression above is exactly the residue of the S matrix or T matrix,

$$\mathrm{Res}|S_{jj}(E)||_{E=E_R}=\left|\frac{\mu_j k_{R,j}}{4\pi^2}\langle k_{R,j}|\hat{V}|\phi\rangle^2\right|, \quad (29)$$

where j stands for the jth channel.

Compared with the LS equation, CSM gives the same information of the positions and residues of the poles, but in a faster and more direct way, since one does not have to numerically search for the poles.

For the narrow resonances away from thresholds, the residue of the S matrix corresponds to the partial width of the resonance,

$$S_{ij}(E)\approx\delta_{i,j}-\frac{i\sqrt{\Gamma_i\Gamma_j}}{E-(M-\frac{i}{2}\Gamma)}. \quad (30)$$

For the resonances near the threshold, Eq. (30) does not hold anymore. The partial widths can be still well defined as the residues of the S matrix, but they no longer add up to the total width. In this work, we only use Eq. (26) to calculate the branching ratio, which is independent of the choice of the normalization conditions.

V. EFFECTS OF THE THREE-BODY THRESHOLD

In line with Ref. [42], the on-shell intermediate $DD(\bar{D})\pi$ state plays an important role in the width of the T_{cc}^+ and $\chi_{c1}(3872)$. Since the mass splitting between Λ_c and $\Sigma_c^{(*)}$ is larger than the pion mass, we include the effect of the three-body intermediate states in the OPE potential in this work.

Still, we retain the 0-th component of the transferred momentum $q=p-p'$ for the OPE potential

$$V_{1\pi}=-C\frac{(S_1\cdot q)(S_2\cdot q)}{q_0^2-\boldsymbol{q}^2-m_\pi^2+i0+}, \quad (31)$$

where S_1 and S_2 are the spin operators of $\Sigma_c^{(*)}(\Lambda_c)$ and $\bar{D}^{(*)}$, and p, p' represent the center-of-mass momentum of the initial and final state, respectively. C is a constant depending on the isospin and coupling constants.

Different from the DD^* system, the OPE potential in $\Sigma_c^{(*)}(\Lambda_c)\bar{D}^{(*)}$ arises from a direct diagram rather than a cross diagram (see Fig. 3). We choose the q^0 as the form

$$q^0=\sqrt{\vec{p}'^2+m_3^2}-\sqrt{\vec{p}^2+m_1^2}. \quad (32)$$

We start from the 4-dimensional equation

$$\begin{aligned}T_{ij}(\boldsymbol{p}',\boldsymbol{p};p_0',p_0,E)&=V_{ij}(\boldsymbol{p}',\boldsymbol{p};p_0',p_0)\\&+\int\frac{d^4l}{(2\pi)^4}V_{ik}(\boldsymbol{p}',\boldsymbol{l};p_0',l_0)\\&\times\mathcal{G}_k(l;E)T_{kj}(\boldsymbol{l},\boldsymbol{p};l_0,p_0,E).\end{aligned} \quad (33)$$

To avoid ambiguity, we write the 3-momentum $\boldsymbol{p}',\boldsymbol{p}$ and energy p_0',p_0 separately. i,j,k are the channel labels. E is the total energy and is conserved in the initial, intermediate

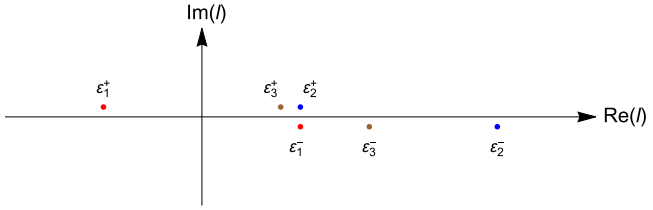

FIG. 4. The poles arise from the integral in Eq. (39). The positions of $\varepsilon_3^\pm$ depend on the mass difference of the initial and final particles. In this figure, the major contributions arise from $\varepsilon_1^-, \varepsilon_2^+$ and ε_3^+. We can perform the integral in the lower half plane and consider only the residue of ε_1^-.

and final states. In general, the T matrices need not be on-shell, namely p_0', p_0, E can be set to any value regardless of $\boldsymbol{p}', \boldsymbol{p}$. But for the on-shell T matrices, all momenta are on-shell and the energies sum up to E, either in the initial or final states.

Then we perform the integral on l^0 using the residue theorem. The propagator of the ith channel reads

$$\mathcal{G}_k(l;E) = \frac{i}{(l^2 - M_{k1}^2 + i\epsilon)[(P-l)^2 - M_{k2}^2 + i\epsilon]}, \tag{34}$$

where M_{k1}, M_{k2} denote the masses of the particles in the kth channel. $P = (E, 0, 0, 0)$ is the total 4-momentum.

Then the poles read

$$\begin{aligned}\varepsilon_1^\pm &= \mp\left(\sqrt{\boldsymbol{l}^2 + M_{k1}^2} - i\epsilon\right) \approx \mp M_{k1},\\ \varepsilon_2^\pm &= E \mp \left(\sqrt{\boldsymbol{l}^2 + M_{k2}^2} - i\epsilon\right) \approx E \mp M_{k2}.\end{aligned} \tag{35}$$

The relative position of the poles are shown in Fig. 4. There is also a pole in $V_{ik}(\boldsymbol{p}', \boldsymbol{l}; p_0', l_0)$, which can be derived from Eq. (31)

$$\varepsilon_3^\pm = p_0' \mp \left(\sqrt{(\boldsymbol{l} - \boldsymbol{p}')^2 + m_\pi^2} - i\epsilon\right) \approx M_{i1} \mp m_\pi \tag{36}$$

The possible poles of the T matrices are not considered. For illustration, we regard Eq. (39) as an analytical extension of T on p_0'-plane [like Eq. (19)] by setting the $\boldsymbol{p}', p_0$ to complex values while the integral on l is performed along the real axis. Obviously, there are no poles of T on the p_0'-plane other than those of V. In fact, we can solve the T matrix formally $T = [1 - VG]^{-1}V$. If we fix the p and E to certain values and discretize the p' or l, then the T matrix will reduce to a "vector". The poles correspond to the zeros of the determinant $|1 - VG|$, where every term of the discretized T vector is divergent. I.e., even a half-on-shell $T(p', p; E)$ matrix (p is on-shell while p' is not) is divergent. The pole structure does not appear on the p_0'-plane but is related to the variable E.

Since we are discussing low energy physics, we suppose the integral on $\boldsymbol{l}$ is regulated in a certain way, so the integral is convergent and 3-momentum is small compared to the masses of the charmed hadrons. Then we can estimate the contributions of the poles.

In general, the far-away poles contribute little to the integral, and we only count the poles with the other poles in their neighborhood. For instance, ε_1^- and ε_2^+ are close to each other since $E \approx M_{k1} + M_{k2}$ in the non-relativistic limit, from which the nonrelativistic form is deduced,

$$\begin{aligned}&\int \frac{d^4l}{(2\pi)^4} V_{ik}(\boldsymbol{p}', \boldsymbol{l}; p_0', l_0)\mathcal{G}_k(l;E)T_{kj}(\boldsymbol{l}, \boldsymbol{p}; l_0, p_0, E)\\ &\to -2\pi \int \frac{d^3l}{(2\pi)^4} \frac{V_{ik}(\boldsymbol{p}', \boldsymbol{l}; p_0', \varepsilon_2^+)T_{kj}(\boldsymbol{l}, \boldsymbol{p}; \varepsilon_2^+, p_0, E)}{(\varepsilon_2^+ - \varepsilon_2^-)(\varepsilon_2^+ - \varepsilon_1^-)(\varepsilon_2^+ - \varepsilon_1^+)},\\ &= \int \frac{d^3l}{(2\pi)^3} \frac{V_{ik}(\boldsymbol{p}', \boldsymbol{l}; p_0', \varepsilon_2^+)T_{kj}(\boldsymbol{l}, \boldsymbol{p}; \varepsilon_2^+, p_0, E)}{4E\sqrt{M_{k2}^2 + \boldsymbol{l}^2}(\sqrt{M_{k2}^2 + \boldsymbol{k}_0^2} - \sqrt{M_{k2}^2 + \boldsymbol{l}^2})},\end{aligned} \tag{37}$$

where the center-of-mass momentum $\boldsymbol{k}_0$ satisfies $E = \sqrt{M_{k1}^2 + \boldsymbol{k}_0^2} + \sqrt{M_{k2}^2 + \boldsymbol{k}_0^2}$. After applying the non-relativistic reduction and considering the normalization constants, we obtain Eq. (13).

The poles ε_1^+ and ε_2^- can be dropped [55] because there is a $(E + M_{k1} + M_{k2})$ in the denominator, and $V_{ik}(\boldsymbol{p}', \boldsymbol{l}; p_0', p_0)$ is small when p_0 deviates from p_0'. However, the poles $\varepsilon_3^\pm$ have a considerable contribution when $\varepsilon_3^\pm$ gets close to ε_2^+ by accident. The condition reads

$$|M_{i1} - M_{k1}| \sim m_\pi, \tag{38}$$

which turns out to be true for the $\Sigma_c - \Lambda_c$ or $D^* - D$ systems.

Instead of directly calculating the residue of $\varepsilon_3^\pm$, we select an appropriate integral contour to include only one pole. For example, if $M_{k1} - M_{i1} \sim m_\pi$, we perform the integral in the upper half plane and consider only ε_2^+. Subsequently, we obtain the 3-dimensional LS equation

$$\begin{aligned}T_{ij}(\boldsymbol{p}', \boldsymbol{p}; p_0', p_0, E) = V_{ij}(\boldsymbol{p}', \boldsymbol{p}; p_0', p_0)\\ + \int \frac{d^3l}{(2\pi)^3} V_{ik}(\boldsymbol{p}', \boldsymbol{l}; p_0', \varepsilon_2^+(\boldsymbol{l}))\\ \times G_k(\boldsymbol{l}; E)T_{kj}(\boldsymbol{l}, \boldsymbol{p}; \varepsilon_2^+(\boldsymbol{l}), p_0, E),\end{aligned} \tag{39}$$

where $G_k(\boldsymbol{l}; E)$ is a 3-dimensional propagator, as seen in Eq. (13). In different channels, the choice of ε_2^+ and ε_1^- can be determined independently. Notably, the T matrix in the left and right sides must have the same form to ensure the LS equation to be an iterative equation. Then p_0' must be set to $\varepsilon_2^+(\boldsymbol{p}')$ [56].

Then an appropriate choice of q_0 in the OPE potential reads

$$q_0 = \begin{cases} \varepsilon_2^+(\boldsymbol{p}') - \varepsilon_2^+(\boldsymbol{p}) = \sqrt{\boldsymbol{p}^2 + M_{k2}^2} - \sqrt{\boldsymbol{p}'^2 + M_{i2}^2}, & M_{k1} - M_{i1} \sim m_\pi, \\ \varepsilon_1^-(\boldsymbol{p}') - \varepsilon_1^-(\boldsymbol{p}) = \sqrt{\boldsymbol{p}'^2 + M_{k1}^2} - \sqrt{\boldsymbol{p}^2 + M_{i1}^2}, & M_{i1} - M_{k1} \sim m_\pi. \end{cases} \tag{40}$$

One can use either of them if the mass difference is far away from the pion mass. If repeating the analysis of the cross diagram in the DD^* system, one will find the appropriate choice of q_0 is always $\pm(E - \sqrt{\boldsymbol{p}^2 + M_D^2} - \sqrt{\boldsymbol{p}'^2 + M_D^2})$, as presented in Ref. [42], which indicates that it is the $DD\pi$ intermediate state, rather than $D^*D^*\pi$, that is important.

When $q_0 > m_\pi$, there is a singularity in the OPE potential, which results in a right-hand (unitary) cut. It is related to the on-shell three-body intermediate state according to the optical theorem. As shown in Fig. 5, we use a nonzero complex scaling angle θ to skip the singularity and perform the integral in the 2nd Riemann sheet with respect to the three-body threshold.

VI. EFFECTIVE POTENTIAL

Compared with the Born approximation in the scattering, the effective potential is related to the Feynman amplitude of the two-particle-irreducible diagrams

$$V = -\frac{1}{4}\mathcal{M}, \tag{41}$$

where the factor $-\frac{1}{4}$ differs from the usual $-\prod_i \frac{1}{\sqrt{2M_i}}$ because of the normalization of the heavy meson and baryon fields.

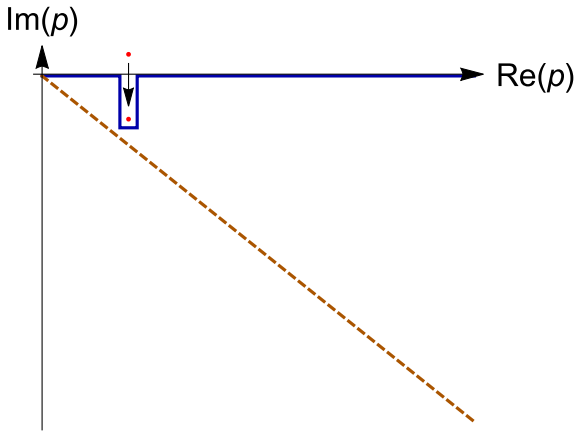

FIG. 5. The integral path from 0 to ∞ in the complex p-plane. The red point denotes the pole of the OPE potential located at $p = \sqrt{p_0^2 - m_\pi^2}$. When the pole passes across the positive real axis, we need to change the integral path to maintain the analytical continuity (blue solid line). Instead, we can carry out a complex scaled integral (brown dashed line) to deal with the pole.

We adopt a Gaussian regulator to suppress the potential V at large momentum p, p', which reads

$$\mathcal{F}(\boldsymbol{p}, \boldsymbol{p}') = \exp\left[-(\boldsymbol{p}^2 + \boldsymbol{p}'^2)/\Lambda^2\right]. \tag{42}$$

We demand $\mathcal{F}(\boldsymbol{p}, \boldsymbol{p}') \to 0$ when $\boldsymbol{p}, \boldsymbol{p}' \to \infty$ before and after the rotation in the complex plane to ensure that the Schrödinger equation can be solved numerically, which constrains the rotating angle $\theta < \pi/4$.

A coupled-channel calculation is performed to investigate the mass and width of the P_c states. The channels considered are listed in Table II. In this work, only the $I = \frac{1}{2}$ channels are considered. The masses and widths of the particles are listed in Table III. We use an average mass for an isospin multiplet. We do not consider the effect of their widths, although they contribute to the width of the P_c states. Apart from the Σ_c^*, the width of the other charmed hadrons is no more than 2 MeV. Since the P_c states are below the nearest thresholds, the off-shell width of Σ_c is smaller than its on-shell value. In this work, we leave it as systematic uncertainties.

The LO contact terms have been investigated in many previous works [28,34,36,37]. We adopt the notations in Ref. [37] and rewrite the contact terms in Tables IV and V for simplification. The extra i arises from the relative phase

TABLE II. The channels considered in the $\Sigma_c^{(*)}(\Lambda_c)\overline{D}^{(*)}$ systems ($I = \frac{1}{2}$).

	1	2	3	4	5
$J^P = \frac{1}{2}^-$	$\Lambda_c\bar{D}$	$\Lambda_c\bar{D}^*$	$\Sigma_c\bar{D}$	$\Sigma_c\bar{D}^*$	$\Sigma_c^*\bar{D}^*$
$J^P = \frac{3}{2}^-$	$\Lambda_c\bar{D}^*$	$\Sigma_c\bar{D}^*$	$\Sigma_c^*\bar{D}$	$\Sigma_c^*\bar{D}^*$	

TABLE III. The masses and widths of the charmed baryons and mesons (MeV). "–" means long-life particles whose width can be ignored [30].

Baryons	Mass	Width	Mesons	Mass	Width
Λ_c^+	2286.46	–	D^-	1869.66	–
Σ_c^{++}	2453.97	1.89	$\bar{D}^0$	1864.84	–
Σ_c^+	2452.65	2.3	D^{*-}	2010.26	8.34×10^{-2}
Σ_c^0	2453.75	1.83	$\bar{D}^{*0}$	2006.85	<2.1
Σ_c^{*++}	2518.41	14.78			
Σ_c^{*+}	2517.4	17.2			
Σ_c^{*0}	2518.48	15.3			

TABLE IV. The contact terms for the $J^P = \frac{1}{2}^-$ channels.

$1/2^-$	$\Lambda_c D$	$\Lambda_c \bar{D}^*$	$\Sigma_c \bar{D}$	$\Sigma_c \bar{D}^*$	$\Sigma_c^* \bar{D}^*$
$\Lambda_c \bar{D}$	A	0	0	$\sqrt{3}iB$	$\sqrt{6}iB$
$\Lambda_c \bar{D}^*$		A	$-\sqrt{3}iB$	$-2B$	$\sqrt{2}B$
$\Sigma_c \bar{D}$			C_a	$\frac{2}{\sqrt{3}}iC_b$	$-\sqrt{\frac{2}{3}}iC_b$
$\Sigma_c \bar{D}^*$				$C_a - \frac{4}{3}C_b$	$-\frac{\sqrt{2}}{3}C_b$
$\Sigma_c^* \bar{D}^*$					$C_a - \frac{5}{3}C_b$

TABLE V. The contact terms for the $J^P = \frac{3}{2}^-$ channels.

$3/2^-$	$\Lambda_c \bar{D}^*$	$\Sigma_c^* \bar{D}$	$\Sigma_c \bar{D}^*$	$\Sigma_c^* \bar{D}^*$
$\Lambda_c \bar{D}^*$	A	$\sqrt{3}iB$	B	$\sqrt{5}B$
$\Sigma_c^* \bar{D}$		C_a	$\frac{iC_b}{\sqrt{3}}$	$\sqrt{\frac{5}{3}}iC_b$
$\Sigma_c \bar{D}^*$			$C_a + \frac{2}{3}C_b$	$-\frac{\sqrt{5}}{3}C_b$
$\Sigma_c^* \bar{D}^*$				$C_a - \frac{2}{3}C_b$

of $\bar{D}$ and $\bar{D}^*$ in the definition of the superfield. The matrix is Hermitian and the lower half of the table is omitted. The constant A and B correspond to C_1 and C_2 in Eq. (11). C_a corresponds to C_3 and C_5. C_b corresponds to C_4 and C_6. We determine the LECs by fitting the masses and widths of the P_c states.

Since we consider only the S-wave interactions, the OPE potential can be written in an equivalent form,

$$V_{1\pi} = -C\frac{(S_1\cdot q)(S_2\cdot q)}{q_0^2-\boldsymbol{q}^2-m_\pi^2+i0+} \to -C\frac{\frac{1}{3}\boldsymbol{q}^2(S_1\cdot S_2)}{q_0^2-\boldsymbol{q}^2-m_\pi^2+i0+}, \tag{43}$$

where S_1 and S_2 are the vectors related to the spin operators of the $\Sigma_c^{(*)}(\Lambda_c)$ or the $\bar{D}^{(*)}$.

In Tables VI and VII, we list the coefficients C_{ij} of the OPE potentials. q_0 for the different channels is determined to be the energy difference of $\Sigma_c^{(*)}$ or Λ_c in the initial and final states. The coefficient matrix is symmetric and the lower half of the table is omitted. C_{ij} is defined as

TABLE VI. The coefficients C_{ij} of the OPE potential for $J^P = \frac{1}{2}^-$ channels.

$1/2^-$	$\Lambda_c D$	$\Lambda_c \bar{D}^*$	$\Sigma_c \bar{D}$	$\Sigma_c \bar{D}^*$	$\Sigma_c^* \bar{D}^*$
$\Lambda_c \bar{D}$	0	0	0	$\frac{\sqrt{6}}{12}igg_2$	$\frac{\sqrt{3}}{6}igg_2$
$\Lambda_c \bar{D}^*$		0	$-\frac{\sqrt{6}}{12}igg_2$	$-\frac{\sqrt{2}}{6}gg_2$	$\frac{1}{6}gg_2$
$\Sigma_c \bar{D}$			0	$\frac{\sqrt{3}}{9}igg_1$	$-\frac{\sqrt{6}}{18}igg_1$
$\Sigma_c \bar{D}^*$				$-\frac{2}{9}gg_1$	$-\frac{\sqrt{2}}{18}gg_1$
$\Sigma_c^* \bar{D}^*$					$-\frac{5}{18}gg_1$

TABLE VII. The coefficients C_{ij} of the OPE potential for $J^P = \frac{3}{2}^-$ channels.

$3/2^-$	$\Lambda_c \bar{D}^*$	$\Sigma_c^* \bar{D}$	$\Sigma_c \bar{D}^*$	$\Sigma_c^* \bar{D}^*$
$\Lambda_c \bar{D}^*$	0	$-\frac{\sqrt{6}}{12}gg_2$	$\frac{\sqrt{2}}{12}gg_2$	$\frac{\sqrt{10}}{12}gg_2$
$\Sigma_c^* \bar{D}$		0	$\frac{\sqrt{3}}{18}igg_1$	$\frac{\sqrt{15}}{18}igg_1$
$\Sigma_c \bar{D}^*$			$\frac{1}{9}gg_1$	$-\frac{\sqrt{5}}{18}gg_1$
$\Sigma_c^* \bar{D}^*$				$-\frac{1}{9}gg_1$

$$V_{1\pi,ij} = C_{ij}\frac{1}{f_\pi^2}\frac{\boldsymbol{q}^2}{-q_0^2+\boldsymbol{q}^2+m_\pi^2-i0+}. \tag{44}$$

VII. NUMERICAL RESULTS AND DISCUSSIONS

A. Fitting the LECs

We discretize Eq. (14) in momentum space to derive the eigenenergies, which corresponds to the pole position of the P_c states. In this work, the $P_c(4312)$ is assigned to a $\frac{1}{2}^-$ $\Sigma_c\bar{D}$ state. The $P_c(4440)$ and $P_c(4457)$ are assigned to the $\frac{1}{2}^-$ and $\frac{3}{2}^-$ $\Sigma_c\bar{D}^*$ states. As shown in Table VI, the OPE potential is attractive in $\frac{1}{2}^-$ channel but repulsive in $\frac{3}{2}^-$ channel. So we prefer to assign the $P_c(4440)$ to the $\frac{1}{2}^-$ channel. The fit under the opposite assignment is shown in the Appendix.

In our fits, the cutoff Λ is fixed to 500 MeV, and there are four LECs to be determined. However, the LEC A only appears in the diagonal terms of the $\Lambda_c\bar{D}^{(*)}$ channel. It weakly affects the masses and widths through the coupled-channel effects. Thus the fit is not sensitive to A. On the other hand, A is important to determine whether the $\Lambda_c\bar{D}^{(*)}$ systems are bound. Thus we adopt two fitting strategies: (1) setting $A = 0$; (2) letting A varies to find the best fit.

The statistical uncertainties in the tables are estimated by the condition $\chi^2 \leq \frac{1+\text{d.o.f.}}{\text{d.o.f.}}\chi_0^2$, where χ_0^2 stands for the minimum of χ^2. The pole positions in Table VIII are derived from the optimal set of LECs.

Table VIII shows the results when we assign $P_c(4440)$ to $\frac{1}{2}^-$ and $P_c(4457)$ to $\frac{3}{2}^-$. In this case, C_a plays a major role while the other LECs are relatively small. The C_a term provides an attractive central potential to bind the $\Sigma_c^{(*)}$ and $\bar{D}$, while the OPE potential provides the coupled-channel interactions and introduces the spin splitting between the $P_c(4440)$ and $P_c(4457)$. Since the OPE potential in $J^P = \frac{3}{2}^-$ $\Sigma_c\bar{D}^*$ system is repulsive, its mass is larger. A similar relationship shows up in the $\Sigma_c^*\bar{D}^*$ system. There are bound states in both $\frac{3}{2}^-$ and $\frac{1}{2}^-$ channels, and the energy of the $\frac{3}{2}^-$ state is higher. Their mass splitting is of the same order of magnitude as the mass splitting between the $P_c(4440)$ and $P_c(4457)$.

In Fit 2, the best fit reveals a large negative A. This results in a bound $\Lambda_c\bar{D}^{(*)}$ state, while the influence on the

TABLE VIII. The fitting result when assigning $P_c(4440)$ to $\frac{1}{2}^-$ and $P_c(4457)$ to $\frac{3}{2}^-$. The units for LECs are GeV^{-2}, and the units for the pole positions ($M - \frac{i\Gamma}{2}$) and cutoff Λ are MeV. The quantum numbers and main components are listed in parentheses.

	Fit 1	Fit 2
χ^2/d.o.f	1.13	1.08
Λ	500	500
A	0	-32^{+15}_{-50}
B	$2.3^{+5.6}_{-3.8}$	-0.3^{+5}_{-5}
C_a	$-53.0^{+3.0}_{-3.0}$	-59.0^{+8}_{-6}
C_b	$1.3^{+2.2}_{-4.8}$	4.3^{+3}_{-10}
$P_c(4312)$	$4309.4 - 3.8i(\Sigma_c\bar{D}, \frac{1}{2}^-)$	$4312.4 - 5.1i(\Sigma_c\bar{D}, \frac{1}{2}^-)$
$P_c(4440)$	$4443.4 - 1.6i(\Sigma_c\bar{D}^*, \frac{1}{2}^-)$	$4438.7 - 1.8i(\Sigma_c\bar{D}^*, \frac{1}{2}^-)$
$P_c(4457)$	$4458.6 - 0.5i(\Sigma_c\bar{D}^*, \frac{3}{2}^-)$	$4457.6 - 0.9i(\Sigma_c\bar{D}^*, \frac{3}{2}^-)$
		$4158.1 - 0.3i(\Lambda_c\bar{D}, \frac{1}{2}^-)$
		$4288.4 - 0.8i(\Lambda_c\bar{D}^*, \frac{1}{2}^-)$
Other states	$4377.8 - 1.6i(\Sigma_c^*\bar{D}, \frac{3}{2}^-)$	$4292.6 - 1.7i(\Lambda_c\bar{D}^*, \frac{3}{2}^-)$
	$4503.9 - 0.5i(\Sigma_c^*\bar{D}^*, \frac{1}{2}^-)$	$4375.4 - 1.8i(\Sigma_c^*\bar{D}, \frac{3}{2}^-)$
	$4516.0 - 1.6i(\Sigma_c^*\bar{D}^*, \frac{3}{2}^-)$	$4497.2 - 0.9i(\Sigma_c^*\bar{D}^*, \frac{1}{2}^-)$
		$4513.0 - 2.6i(\Sigma_c^*\bar{D}^*, \frac{3}{2}^-)$

observed P_c states is small. The widths of the $\Lambda_c\bar{D}^{(*)}$ molecules arise from the imaginary part of the OPE potentials, which is probably overestimated in our approximation. Comparing Fit 1 and Fit 2, we conclude that the coupled-channel interactions from OPE between $\Lambda_c\bar{D}^{(*)}$ and $\Sigma_c\bar{D}^{(*)}$ are not sufficient to generate a $\Lambda_c\bar{D}^{(*)}$ bound state. Nevertheless, if the interaction in $\Lambda_c\bar{D}^{(*)}$ system is attractive enough, there may exist three additional narrow states.

The total width of $P_c(4312)$ is the largest, which physically arises from the strong coupling and proximity of the $\Lambda_c\bar{D}^*$ and $\Sigma_c\bar{D}$ channels. This differs from the center value of the experimental result. One reason is the uncertainties for the experimental widths are large, especially for $P_c(4440)$. This reduces the weight of the width of $P_c(4440)$ in the fit. Another important reason is that the width of Σ_c is not included in the calculation, which may influence the width of the P_c state by 1 to 2 MeV. For the states with Σ_c^*, the width may increase by 10 MeV.

In contrast, the width of the $\frac{1}{2}^-$ $\Sigma_c\bar{D}^*$ bound state is small (except for the effect of the width of $\Sigma_c^{(*)}$), although it is strongly coupled to the $\frac{1}{2}^-$ $\Lambda_c\bar{D}$ channel and the phase space is large. It indicates the influence from a relatively far threshold is small. Since the momentum in the lower channel could be large and the potential could be suppressed by the regulator, it is not quite reasonable to consider the far-away thresholds in a nonrelativistic framework.

In all fits, we find the $J^P = \frac{3}{2}^-$ states near the $\Sigma_c^*\bar{D}$ and the $\Sigma_c^*\bar{D}^*$ thresholds always exist. They are on the 1st Riemann sheet with respect to the $\Sigma_c^*\bar{D}^{(*)}$ threshold. The former corresponds to the previously reported $P_c(4380)$ and the latter is predicted to be located in the vicinity of 4520 MeV, whose width could be much larger than our results since Σ_c^* has a large width.

B. Partial width

The interaction between Λ_c and $\bar{D}^{(*)}$ is believed to be weak because the spin and the isospin of the light quarks in Λ_c are both zero. Through a S-wave interaction, they can be coupled only to isospin-0 scalar mesons. Thus we choose Fit 1 to calculate the branching ratios, root-mean-square (rms) radii and component proportions of the P_c states. The uncertainties are estimated in the domain $\chi^2 \leq \frac{1+\text{d.o.f.}}{\text{d.o.f.}}\chi_0^2$. The uncertainties of $P_c(4312)$, $P_c(4440)$, and $P_c(4457)$ are similar to the experimental uncertainties due to the fit, and the uncertainties of widths are large.

The rms radius and the component proportion are defined by the c-product [57]

$$(\psi|r^2|\psi) = \sum_i \int r^2\psi_i(\boldsymbol{r})^2 d^3\boldsymbol{r},$$
$$(\psi_i|\psi_i) = \int \psi_i(\boldsymbol{r})^2 d^3\boldsymbol{r}, \tag{45}$$

in which the wave function of the ith channel ψ_i satisfies the normalization condition

$$\sum_i (\psi_i|\psi_i) = 1. \tag{46}$$

In the c-product, the inner product is defined using the square of the wave function rather than the square of its modulus. Although $\psi_i(r)$ is divergent at infinity in open channels, the integral in Eq. (45) can be defined using analytical extension, and is generally not real.

As shown in Table IX, the imaginary part of the rms radius is small, which indicates the state is similar to the stable states. The rms radii are of the order of magnitude of 1 fm and qualitatively in proportion to the inverse of the binding energies, which is in accordance with the molecular state assumption.

All the states are found to be the quasibound states. In other words, the momenta with respect to the higher thresholds have positive imaginary parts, which results in convergent wave functions in coordinate space, while it is opposite for the lower thresholds. In the higher channels, the pole is on the 1st Riemann sheet and the divergent term of Eq. (22) vanishes. The wave function is similar to that of the bound states, which implies the possibility of finding two free particles in infinity is zero. Although the residue of the T matrix in Eq. (30) may be large, the state will not decay to the corresponding channel. Thus, when we evaluate the branching ratios, only the lower channels, of which the pole lies on the 2nd Riemann sheet, are considered. The three-body decays are partly included in the total width, but not considered in the branching ratios.

TABLE IX. The root-mean-square radii and open-charm branching ratios of the P_c states. LECs in Fit 1 are adopted. The unit for M and Γ is MeV, the unit for RMS radii is fm, and the unit for the branching ratios is %. "–" means the state will not decay to the channel.

$\frac{1}{2}^-$	$P_c(4312)$	$P_c(4440)$	$P_c(4504)$
M	$4309.4^{+2.7}_{-2.5}$	$4443.5^{+3.7}_{-3.5}$	$4504.0^{+6.1}_{-4.7}$
Γ	$7.8^{+6.6}_{-6.6}$	$3.1^{+0.8}_{-1.4}$	$1.5^{+0.4}_{-1.4}$
$M_{\rm exp}$	$4311.9 \pm 0.7^{+6.8}_{-0.6}$	$4440.3 \pm 1.3^{+4.1}_{-4.7}$	
$\Gamma_{\rm exp}$	$9.8 \pm 2.7^{+3.7}_{-4.5}$	$20.6 \pm 4.9^{+8.7}_{-10.1}$	
$\sqrt{(\phi_i\|r^2\|\phi_i)}$	$0.63 - 0.11i^{+0.07+0.09i}_{-0.07-0.09i}$	$0.60 - 0.01i^{+0.03+0.01i}_{-0.01-0.00i}$	$0.58 + 0.00i^{+0.03+0.00i}_{-0.01i-0.01i}$
$\Lambda_c\bar{D}$	$0.04^{+0.01}_{-0.02}$	$10.8^{+8.0}_{-2.7}$	$8.7^{+7.0}_{-6.6}$
$\Lambda_c\bar{D}^*$	$99.96^{+0.02}_{-0.01}$	$38.4^{+24.9}_{-30.6}$	$24.6^{+17.1}_{-18.3}$
$\Sigma_c\bar{D}$	–	$50.9^{+38.6}_{-27.4}$	$31.6^{+16.2}_{-14.4}$
$\Sigma_c\bar{D}^*$	–	–	$35.2^{+8.7}_{-9.7}$
$\Sigma_c^*\bar{D}^*$	–	–	–
$\frac{3}{2}^-$	$P_c(4380)$	$P_c(4457)$	$P_c(4516)$
M	$4377.9^{+2.3}_{-3.0}$	$4458.6^{+1.4}_{-2.5}$	$4516.0^{+2.1}_{-2.5}$
Γ	$3.2^{+1.7}_{-3.1}$	$1.0^{+0.3}_{-0.4}$	$3.2^{+1.4}_{-1.7}$
$M_{\rm exp}$		$4457.3 \pm 0.6^{+4.1}_{-1.7}$	
$\Gamma_{\rm exp}$		$6.4 \pm 2.0^{+5.7}_{-1.9}$	
$\sqrt{(\phi_i\|r^2\|\phi_i)}$	$0.74 - 0.03i^{+0.06+0.02i}_{-0.06-0.02i}$	$0.84 + 0.01i^{+0.08+0.01i}_{-0.08-0.01i}$	$0.67 - 0.01i^{+0.03+0.01i}_{-0.02-0.01i}$
$\Lambda_c\bar{D}^*$	100	$26.9^{+30.0}_{-22.5}$	$18.1^{+23.7}_{-14.5}$
$\Sigma_c^*\bar{D}$	–	$73.1^{+22.5}_{-30.0}$	$45.6^{+7.9}_{-13.1}$
$\Sigma_c\bar{D}^*$	–	–	$36.2^{+6.6}_{-10.6}$
$\Sigma_c^*\bar{D}^*$	–	–	–

Although the branching ratios in different channels are mostly comparable, the $P_c(4312)$ is an exception. The state decays mainly to the $\Lambda_c\bar{D}^*$ channel, while the decay to the $\Lambda_c\bar{D}$ channel is suppressed since the OPE potential vanishes in the $\Lambda_c\bar{D}^* \to \Lambda_c\bar{D}$ or $\Sigma_c\bar{D} \to \Lambda_c\bar{D}$. In disregard of the uncertainties, the branching ratios to the closer channels are likely to be larger. For the $P_c(4457)$, the branching ratio to the $\Sigma_c^*\bar{D}$ channel is larger. For the $P_c(4440)$ and $P_c(4504)$, the branching ratios to the $\Lambda_c\bar{D}^*$ channel are relatively small.

We further calculate the proportion of components using the probability defined by c-product and the results are listed in Table X. The $P_c(4312)$ shows a mixing of $\Lambda_c\bar{D}^*$ and $\Sigma_c\bar{D}$, while the other states are nearly a single-channel bound state. Since they are bound states in the corresponding channels, they can only decay to the lower channels.

TABLE X. The components of the P_c states. The probability in the ith channel is defined by the c-product $(\phi_i|\phi_i)$ and hence has an imaginary part. The unit is %.

$\frac{1}{2}^-$	$P_c(4312)$	$P_c(4440)$	$P_c(4504)$
$\Lambda_c\bar{D}$	$0.00^{+0.00}_{-0.00}$	$0.07 + 0.01i^{+0.03+0.00i}_{-0.06-0.00i}$	$0.06 + 0.07i^{+0.03+0.02i}_{-0.06-0.04i}$
$\Lambda_c\bar{D}^*$	$\mathbf{5.3 - 0.5i}^{+5.5+3.9i}_{-4.6-0.9i}$	$0.14 - 0.01i^{+0.10+0.01i}_{-0.12-0.01i}$	$0.08 + 0.05i^{+0.05+0.00i}_{-0.07-0.02i}$
$\Sigma_c\bar{D}$	$\mathbf{94.5 + 0.2i}^{+4.6+0.9i}_{-5.5-4.1i}$	$0.11 + 0.04i^{+0.08+0.02i}_{-0.08-0.03i}$	$0.07 - 0.02i^{+0.06+0.02i}_{-0.05-0.01i}$
$\Sigma_c\bar{D}^*$	$0.2 + 0.3i^{+0.1+0.2i}_{-0.2-0.3i}$	$\mathbf{99.1 + 0.2i}^{+0.5+0.1i}_{-0.4-0.1i}$	$0.09 + 0.22i^{+0.04+0.18i}_{-0.07-0.16i}$
$\Sigma_c^*\bar{D}^*$	$0.02 + 0.05i^{+0.03+0.05i}_{-0.04-0.04i}$	$0.6 - 0.2i^{+0.4+0.1i}_{-0.4-0.1i}$	$\mathbf{99.7 - 0.3i}^{+0.2+0.2i}_{-0.1-0.2i}$
$\frac{3}{2}^-$	$P_c(4380)$	$P_c(4457)$	$P_c(4516)$
$\Lambda_c\bar{D}^*$	$0.24 + 0.17i^{+0.12+0.08i}_{-0.21-0.06i}$	$0.01 + 0.00i^{+0.01+0.01i}_{-0.01-0.00i}$	$0.03 + 0.08i^{+0.05+0.02i}_{-0.04-0.05i}$
$\Sigma_c^*\bar{D}$	$\mathbf{99.6 - 0.3i}^{+0.2+0.2i}_{-0.3-0.1i}$	$0.01 + 0.01i^{+0.01+0.02i}_{-0.01-0.01i}$	$0.08 + 0.03i^{+0.05+0.03i}_{-0.05-0.03i}$
$\Sigma_c\bar{D}^*$	$0.08 + 0.06i^{+0.13+0.03i}_{-0.08-0.05i}$	$\mathbf{99.92 - 0.07i}^{+0.04+0.04i}_{-0.09-0.06i}$	$0.07 + 0.09i^{+0.05+0.08i}_{-0.05-0.07i}$
$\Sigma_c^*\bar{D}^*$	$0.10 + 0.07i^{+0.19+0.04i}_{-0.10-0.06i}$	$0.06 + 0.05i^{+0.08+0.05i}_{-0.03-0.03i}$	$\mathbf{99.81 - 0.19i}^{+0.09+0.09i}_{-0.06-0.09i}$

The $P_c(4380)$ is a molecule of the $\Sigma_c^*\bar{D}$. The $P_c(4440)$ and $P_c(4457)$ are the molecules of $\Sigma_c\bar{D}^*$. The $P_c(4504)$ and $P_c(4516)$ are the molecules of $\Sigma_c^*\bar{D}^*$. The branching ratios are derived from the probabilities.

VIII. SUMMARY

We perform a deduction of the analytical extension of wave functions in momentum space. Then the analytical behavior of the wave function in coordinate space is obtained using the Fourier transformation. We show how CSM works from the point of view of analytical extension. Whether we include the residue of the pole of the wave function in the integral or not will affect which Riemann sheet the pole is located on. In this way, the branching ratio is derived from the complex wave function. Such a formalism can be easily extended to other systems.

In order to make use of the experimental values of the widths of the P_c states, we have performed a coupled-channel analysis using CSM. The potential arises from OPE involving the on-shell three-body intermediate states and contact terms with undetermined LECs. We use the masses and widths of the $P_c(4312)$, $P_c(4440)$, $P_c(4457)$ as inputs to fit the LECs. Then we calculate the branching ratios of the open-charm two-body final states of the observed P_c states and other predicted states.

Assuming the coupled-channel effects arise mainly from OPE, which implies the LECs B and C_b are small, we prefer to assign the $P_c(4440)$ to $\frac{1}{2}^-$ and the $P_c(4457)$ to $\frac{3}{2}^-$. Under this assignment, three additional states are obtained at the vicinity of 4380 MeV, 4504 MeV and 4516 MeV, which are mainly the bound states of $\Sigma_c^*\bar{D}^{(*)}$. The mass splitting of the latter two states is similar to that of the $P_c(4440)$ and $P_c(4457)$, whereas their widths may be larger than our prediction because of the large width of the Σ_c^*. If we interchange the assignment, the $\frac{1}{2}^-$ $\Sigma_c^*\bar{D}^*$ may not be bound. Since the observed P_c states depend weakly on the LEC A, its value is unlikely to be determined. However, a large negative A in the best fit will result in extra states which are mainly $\Lambda_c\bar{D}^*$ bound states. Given that the interactions in the $\Lambda_c\bar{D}$ system are weak in meson-exchange models, we force A to be zero and calculate the branching ratios.

Our result shows that all the states are the quasibound states near the physical region. The $P_c(4312)$ has considerable proportions in the $\Lambda_c\bar{D}^*$ and $\Sigma_c\bar{D}$ channels. It lies on the 1st Riemann sheet with respect to the $\Sigma_c\bar{D}$ threshold and the 2nd Riemann sheet with respect to the $\Lambda_c\bar{D}^*$ threshold. It decays mainly to $\Lambda_c\bar{D}^*$ rather than $\Lambda_c\bar{D}$. Other states are mainly the bound states of the closest channel, and decay only to the lower channels. The branching ratios of decaying to the closer channels tend to be larger. These channels will be helpful to search for the P_c states.

ACKNOWLEDGMENTS

This work is supported by the National Natural Science Foundation of China under Grants No. 11975033, No. 12070131001 and No. 12147168. The authors thank Yan-Ke Chen and Liang-Zhen Wen for helpful discussions.

APPENDIX: INTERCHANGING THE SPIN ASSIGNMENTS

Table XI shows the result when we assign $P_c(4440)$ to $\frac{3}{2}^-$ and $P_c(4457)$ to $\frac{1}{2}^-$. In this case, C_b becomes important because it reverses the spin splitting between the $\frac{3}{2}^-$ and $\frac{1}{2}^-$ states. One remarkable feature is that C_b introduces a large repulsive potential in the $\frac{1}{2}^-$ $\Sigma_c^*\bar{D}^*$ channel, and they are not bound anymore. There will be only one state around the $\Sigma_c^*\bar{D}^*$ threshold with $J^P = \frac{3}{2}^-$. However, if we allow A to vary, there will be the $\Lambda_c\bar{D}^*$ bound states, and their mass splitting will not be reversed since C_b is in the $\Sigma_c^{(*)}$ sector.

TABLE XI. The fitting result when assigning $P_c(4440)$ to $\frac{3}{2}^-$ and $P_c(4457)$ to $\frac{1}{2}^-$. The $\frac{1}{2}^-$ $\Sigma_c^*\bar{D}^*$ system is not bound. The units for LECs are GeV^{-2}, and the units for the pole positions ($M - \frac{i\Gamma}{2}$) are MeV. The quantum numbers and main components are listed in parentheses.

	Fit 3	Fit 4
χ^2/d.o.f	1.58	0.92
Λ	500	500
A	0	-38.3^{+15}_{-20}
B	$-0.1^{+6.1}_{-2.8}$	$-8.8^{+5.4}_{-4.1}$
C_a	$-55.4^{+4.7}_{-3.9}$	$-67.1^{+5.0}_{-4.3}$
C_b	$-30.2^{+5.0}_{-4.7}$	$-28.3^{+5.2}_{-3.8}$
$P_c(4312)$	$4308.2 - 3.5i(\Sigma_c\bar{D}, \frac{1}{2}^-)$	$4311.9 - 4.9i(\Sigma_c\bar{D}, \frac{1}{2}^-)$
$P_c(4440)$	$4446.7 - 0.5i(\Sigma_c\bar{D}^*, \frac{3}{2}^-)$	$4439.1 - 0.8i(\Sigma_c\bar{D}^*, \frac{3}{2}^-)$
$P_c(4457)$	$4458.4 - 1.8i(\Sigma_c\bar{D}^*, \frac{1}{2}^-)$	$4457.4 - 3.6i(\Sigma_c\bar{D}^*, \frac{1}{2}^-)$
		$4154.2 - 0.6i(\Lambda_c\bar{D}, \frac{1}{2}^-)$
		$4277.1 - 0.8i(\Lambda_c\bar{D}^*, \frac{1}{2}^-)$
Other states	$4377.5 - 1.6i(\Sigma_c^*\bar{D}, \frac{3}{2}^-)$	$4285.9 - 2.2i(\Lambda_c\bar{D}^*, \frac{3}{2}^-)$
	$4526.7 - 0.2i(\Sigma_c^*\bar{D}^*, \frac{3}{2}^-)$	$4372.7 - 1.8i(\Sigma_c^*\bar{D}, \frac{3}{2}^-)$
		$4524.5 - 1.4i(\Sigma_c^*\bar{D}^*, \frac{3}{2}^-)$
		$4526.9 - 0.3i(\Sigma_c^*\bar{D}^*, \frac{1}{2}^-)$

[1] H.-X. Chen, W. Chen, X. Liu, and S.-L. Zhu, Phys. Rep. **639**, 1 (2016).
[2] R. F. Lebed, R. E. Mitchell, and E. S. Swanson, Prog. Part. Nucl. Phys. **93**, 143 (2017).
[3] S. L. Olsen, T. Skwarnicki, and D. Zieminska, Rev. Mod. Phys. **90**, 015003 (2018).
[4] F.-K. Guo, C. Hanhart, U.-G. Meißner, Q. Wang, Q. Zhao, and B.-S. Zou, Rev. Mod. Phys. **90**, 015004 (2018); **94**, 029901(E) (2022).
[5] Y.-R. Liu, H.-X. Chen, W. Chen, X. Liu, and S.-L. Zhu, Prog. Part. Nucl. Phys. **107**, 237 (2019).
[6] N. Brambilla, S. Eidelman, C. Hanhart, A. Nefediev, C.-P. Shen, C. E. Thomas, A. Vairo, and C.-Z. Yuan, Phys. Rep. **873**, 1 (2020).
[7] H.-X. Chen, W. Chen, X. Liu, Y.-R. Liu, and S.-L. Zhu, Rep. Prog. Phys. **86**, 026201 (2023).
[8] L. Meng, B. Wang, G.-J. Wang, and S.-L. Zhu, Phys. Rep. **1019**, 1 (2023).
[9] T. Gershon (LHCb Collaboration), arXiv:2206.15233.
[10] R. Aaij *et al.* (LHCb Collaboration), Phys. Rev. Lett. **115**, 072001 (2015).
[11] R. Aaij *et al.* (LHCb Collaboration), Phys. Rev. Lett. **117**, 082002 (2016).
[12] R. Aaij *et al.* (LHCb Collaboration), Phys. Rev. Lett. **122**, 222001 (2019).
[13] R. Aaij *et al.* (LHCb Collaboration), Phys. Rev. Lett. **128**, 062001 (2022).
[14] Z.-C. Yang, Z.-F. Sun, J. He, X. Liu, and S.-L. Zhu, Chin. Phys. C **36**, 6 (2012).
[15] J.-J. Wu, R. Molina, E. Oset, and B. S. Zou, Phys. Rev. Lett. **105**, 232001 (2010).
[16] J.-J. Wu, R. Molina, E. Oset, and B. S. Zou, Phys. Rev. C **84**, 015202 (2011).
[17] E. Hiyama, A. Hosaka, M. Oka, and J.-M. Richard, Phys. Rev. C **98**, 045208 (2018).
[18] X.-Z. Weng, X.-L. Chen, W.-Z. Deng, and S.-L. Zhu, Phys. Rev. D **100**, 016014 (2019).
[19] F.-K. Guo, U.-G. Meißner, W. Wang, and Z. Yang, Phys. Rev. D **92**, 071502(R) (2015).
[20] M. Bayar, F. Aceti, F.-K. Guo, and E. Oset, Phys. Rev. D **94**, 074039 (2016).
[21] S. X. Nakamura, Phys. Rev. D **103**, L111503 (2021).
[22] Y. Yamaguchi, H. García-Tecocoatzi, A. Giachino, A. Hosaka, E. Santopinto, S. Takeuchi, and M. Takizawa, Phys. Rev. D **101**, 091502(R) (2020).
[23] H.-X. Chen, W. Chen, and S.-L. Zhu, Phys. Rev. D **100**, 051501(R) (2019).
[24] J.-J. Wu, T. S. H. Lee, and B. S. Zou, Phys. Rev. C **85**, 044002 (2012).
[25] X.-K. Dong, F.-K. Guo, and B.-S. Zou, Commun. Theor. Phys. **73**, 125201 (2021).
[26] R. Chen, Z.-F. Sun, X. Liu, and S.-L. Zhu, Phys. Rev. D **100**, 011502(R) (2019).
[27] M. I. Eides, V. Y. Petrov, and M. V. Polyakov, Phys. Rev. D **93**, 054039 (2016).
[28] L. Meng, B. Wang, G.-J. Wang, and S.-L. Zhu, Phys. Rev. D **100**, 014031 (2019).
[29] B. Wang, L. Meng, and S.-L. Zhu, J. High Energy Phys. 11 (2019) 108.
[30] R. L. Workman *et al.* (Particle Data Group), Prog. Theor. Exp. Phys. **2022**, 083C01 (2022).
[31] U. Skerbis and S. Prelovsek, Phys. Rev. D **99**, 094505 (2019).
[32] T. Sugiura, Y. Ikeda, and N. Ishii, EPJ Web Conf. **175**, 05011 (2018).
[33] H. Xing, J. Liang, L. Liu, P. Sun, and Y.-B. Yang, arXiv: 2210.08555.
[34] C. W. Xiao, J. Nieves, and E. Oset, Phys. Rev. D **100**, 014021 (2019).
[35] A. Feijoo, W.-F. Wang, C.-W. Xiao, J.-J. Wu, E. Oset, J. Nieves, and B.-S. Zou, Phys. Lett. B **839**, 137760 (2023).
[36] M.-L. Du, V. Baru, F.-K. Guo, C. Hanhart, U.-G. Meißner, J. A. Oller, and Q. Wang, Phys. Rev. Lett. **124**, 072001 (2020).
[37] T. J. Burns and E. S. Swanson, Phys. Rev. D **106**, 054029 (2022).
[38] M.-L. Du, A. Filin, V. Baru, X.-K. Dong, E. Epelbaum, F.-K. Guo, C. Hanhart, A. Nefediev, J. Nieves, and Q. Wang, Phys. Rev. Lett. **131**, 131903 (2023).
[39] M.-L. Du, V. Baru, F.-K. Guo, C. Hanhart, U.-G. Meißner, J. A. Oller, and Q. Wang, J. High Energy Phys. 08 (2021) 157.
[40] N. Moiseyev, P. Certain, and F. Weinhold, Mol. Phys. **36**, 1613 (1978).
[41] T. Myo, Y. Kikuchi, H. Masui, and K. Katō, Prog. Part. Nucl. Phys. **79**, 1 (2014).
[42] Z.-Y. Lin, J.-B. Cheng, and S.-L. Zhu, arXiv:2205.14628.
[43] K. Chen, Z.-Y. Lin, and S.-L. Zhu, Phys. Rev. D **106**, 116017 (2022).
[44] M. B. Wise, Phys. Rev. D **45**, R2188 (1992).
[45] K. Chen, B.-L. Huang, B. Wang, and S.-L. Zhu, arXiv: 2204.13316.
[46] Y.-R. Liu and M. Oka, Phys. Rev. D **85**, 014015 (2012).
[47] J. Aguilar and J. M. Combes, Commun. Math. Phys. **22**, 269 (1971).
[48] E. Balslev and J. M. Combes, Commun. Math. Phys. **22**, 280 (1971).
[49] For example, a transformation $r \to -r$ will not make the bound states divergent or virtual states convergent.
[50] A. M. Badalian, L. P. Kok, M. I. Polikarpov, and Y. A. Simonov, Phys. Rep. **82**, 31 (1982).
[51] T. Noro and H. S. Taylor, J. Phys. B **13**, L377 (1980).
[52] H. Masui, S. Aoyama, T. Myo, and K. Kato, Prog. Theor. Phys. **102**, 1119 (1999).
[53] N. Moiseyev and U. Peskin, Phys. Rev. A **42**, 255 (1990).
[54] W. J. Romo, Nucl. Phys. **A116**, 617 (1968).
[55] For energy-independent potentials, we usually sum up the residues of two poles ϵ_1^+ and ϵ_2^+, but in fact the former is small.
[56] One may notice that $V_{ij}(\boldsymbol{p}', \boldsymbol{p}; p_0', p_0)$ is different from $V_{ik}(\boldsymbol{p}', \boldsymbol{l}; p_0', \epsilon_2^+(\boldsymbol{l}))$. This will not cause problems since the poles depend only on the V in the integral.
[57] M. Homma, T. Myo, and K. Katō, Prog. Theor. Phys. **97**, 561 (1997).